Published in final edited form as:
Anal Chem. 2010 April 15; 82(8): 3139–3145. doi:10.1021/ac9027802.

Combining Scanning Electrochemical Microscopy with Infrared Attenuated Total Reflection Spectroscopy for *In-situ* Studies of Electrochemically Induced Processes

Liqun Wang[1], **Janusz Kowalik**[1], **Boris Mizaikoff**[2], and **Christine Kranz**[2,*]

[1] School of Chemistry and Biochemistry, Georgia Institute of Technology, Atlanta, GA 30332

[2] Institute of Analytical and Bioanalytical Chemistry, University of Ulm, Ulm, GER

The combination of scanning electrochemical microscopy (SECM) with single-bounce attenuated total reflection Fourier-transformed infrared spectroscopy (IR-ATR) has been developed for *in-situ* studies on electrochemically induced processes at IR waveguide surfaces via evanescent field absorption spectroscopy. The feasibility of the combined microelectrochemical FT-IR setup was demonstrated by spectroscopically monitoring microstructured polymer depositions induced via feedback mode SECM using a 25 μm Pt disk ultramicroelectrode (UME). The surface of a ZnSe ATR crystal was initially coated with 2,5-di-(2-thienyl)-pyrrole (SNS) layer, which was then locally polymerized during $Ru(bpy)_3^{2+}$ mediated feedback mode SECM experiments. The polymerization reaction was simultaneously monitored by recording absorption intensity changes of SNS specific IR bands, thereby providing information on the polymerization mechanism, and on the percentage of surface modification.

Introduction

The systematic analysis of processes at the solid/liquid interface requires experimental tools and analytical methods to measure and image qualitatively and quantitatively interfacial events with molecular selectivity, sensitivity, and preferably temporal/spatial resolution. Conventional analytical techniques are frequently limited to bulk averaging measurements or to *ex-situ* analysis. The combination of complementary *in-situ* analytical techniques with scanning probe microscopies (SPM) enables bridging this gap for elucidating fundamental processes at the solid/liquid interface.

Among the scanning probe techniques, SECM has matured into a versatile *in-situ* technique providing information on homogeneous and heterogeneous electron transfer mechanism at solid/liquid, liquid/liquid, and air/liquid interfaces.1, 2 In addition, SECM has successfully been used for microstructuring surfaces using deposition or etching processes.3 Either direct mode of SECM using an ultramicroelectrode (UME) as auxiliary electrode and the biased sample as working electrode, or feedback mode experiments at conductive and insulating sample have been described in literature.4–22 First approaches using the direct mode for microstructuring were based on applying a bias between an electrochemical scanning tunneling microscope (STM) tip, and a conductive surface, which was covered with a thin polymer film such as e.g., Nafion.21, 22 The localized current established between tip and sample was responsible for reducing or oxidizing metal ions or organic ions incorporated in the film, thereby forming metal lines or polymer lines. Furthermore, direct mode deposition of 2- and

*Corresponding author: christine.kranz@uni-ulm.de.

3-dimenional polymer structures using pulsed deposition profiles has also been achieved using disk-shaped microelectrodes as auxiliary electrodes.[7, 8, 23] The possibly close distance between tip and sample surface, as well as the tip size and geometry governs the dimensions of the obtained microstructures by defining the electrical field distribution between tip and conductive sample. Alternatively, surface modifications may be achieved in feedback mode SECM by generating an electroactive species at the UME, which is diffusing to the sample surface governing the surface modification reaction. Thus, pH shifts induced at the UME were used for depositing polymer and metal structures.[4, 24] Heinze and co-workers have described the structured polymerization of 2,5-di-(2-methylpyrrolidin)-thiophene, which was adsorbed onto a substrate surface prior to feedback mode induced polymerization, as the precursor is not soluble in the mediator solution.[25] To date, surface modification using SECM in feedback mode have been achieved by etching and deposition of metals and semiconductors,[11-15, 26] metal oxides,[19, 27] polymers,[8, 22, 23, 28, 29] and organic molecules as well as biomolecules.[9, 16, 17, 30-34]

In recent years, SECM has been combined with a variety of analytical techniques ranging from mass sensitive and optically responsive methods to complementary scanning probe techniques providing laterally and temporally resolved information on interface processes. Combined electrochemical SPM techniques are mainly based on integrating an electroactive area into a SPM tip. Dependent on the physical near field interaction, ESTM-SECM,[35, 36] photoelectrochemical (PEM)-SECM[37], and AFM-SECM[38-41] have been realized. Complementary bulk information on mass changes can be obtained by SECM combined with an electrochemical quartz crystal microbalance (EQCM) simultaneously detecting the generated species by SECM and the associated mass change.[5, 42-44] SECM has also been combined with optical microscopy,[45, 46] with near-field scanning optical microscopy (NSOM),[47] with fluorescence spectroscopy,[48] chemiluminescence techniques,[49-52] and with surface plasmon resonance (SPR).[53] For example, Szunerits *et al* have developed a combined SECM-SPR set-up, obtaining simultaneous SPR images of micropatterned conductive polypyrrole deposited with SECM.[53]

To our best knowledge, the combination of SECM with spectroscopic techniques operating in the mid-infrared (MIR, 3-25 μm) region of the electromagnetic spectrum has not been described yet. Recently, our research group has developed a combined AFM-IR-ATR set-up, which enabled obtaining simultaneous spectroscopic and topographic information on dissolution processes.[54] However, gaining molecular level insight on reactions or interfacial processes via vibrational spectroscopy in the mid-infrared regime, while simultaneously inducing or probing spatially resolved electrochemistry via SECM further expands the applicability of such multifunctional analytical platforms for studying molecular processes in complex environments.

Mid-infrared spectroscopy is based on the excitation of fundamental vibrational modes of molecules, and is among the most powerful techniques for identifying molecular structures. In particular, the fingerprint regime (10-25 μm) of the IR spectrum provides sensitive and distinct characteristic absorption patterns for almost any organic molecule. However, water absorptions are usually a significant problem for *in-situ* IR spectroscopy due to strong absorption bands at 1640 and 3400 cm^{-1}. To minimize this interference, attenuated total reflection infrared spectroscopy (IR-ATR) is the method of choice due to the exquisite surface sensitivity of the obtained signal limited to the penetration depth of the evanescent field.[55] IR radiation coupled into an internal reflection element at angles exceeding the critical angle propagates within this optical waveguide due to total internal reflections. Given a refractive index n_1 of the waveguide, and n_2 of the surrounding medium (with $n_1 > n_2$), an evanescent field penetrates a short distance beyond the interface into the optically rare medium. This evanescent field is characterized by

a field intensity exponentially decaying with distance to the interface, and typical penetration depths in the MIR of a few micrometers (μm) following

$$d_p = \frac{\lambda}{2\pi\sqrt{n_1^2 \sin(\theta) - n_2^2}} \quad (1)$$

with λ as the incident wavelength, n_1 as the refractive index of the ATR waveguide, n_2 as the refractive index of the adjacent medium ($n_1 > n_2$), and θ as the incidence angle at the interface. IR absorbing molecules either adsorbed at the ATR surface or within the evanescent field are therefore spectroscopically adressable.[55] The effect of strong IR absorbers, such as e.g., water, is therefore minimized during IR-ATR measurements as compared to conventional transmission absorption and reflection absorption IR spectroscopy, due to the limited probed volume as determined by the penetration depth of evanescent field. For example, plasma deposition of polymers at the waveguide surface have been studied by IR-ATR.[56]

In the present study, a combined SECM-IR-ATR system is demonstrated enabling *in-situ* IR-ATR monitoring of microstructured polymer spots generated in feedback mode SECM with a 25 μm (diam.) Pt electrode at the ATR waveguide surface. Surface adsorbed 2,5-di-(2-thienyl)-pyrrole (Figure 1a) insoluble in the mediator solution was polymerized by tip-generated $Ru(bpy)_3^{3+}$ similar to the experiments described by Heinze and co-workers (Fig. 1)[25].

Experimental section

Combined SECM-IR-ATR set-up

A scheme of the developed set-up is shown in Fig. 1. For IR-ATR spectroscopy, broadband IR radiation emitted by a SiC filament from a FT-IR spectrometer (IRCube-M, Bruker Optics Inc., Billerica, MA) is collimated and focused by an off-axis parabolic mirror (OAPM) onto the curvature of a single-bounce hemispherical ZnSe ATR crystal (3 mm in diameter, Harrick Scientific, Pleasantville, NY). Due to the hemispherical shape of the ATR crystal the incident radiation is focused onto a small spot at the flat top surface of the ATR crystal creating the evanescent field. The internally reflected radiation is then collimated via a second OAPM, and focused via a third OAPM onto a liquid nitrogen cooled mercury-cadmium-telluride (MCT) detector. For combined SECM experiments, the ATR crystal has been built into an electrochemical cell as central part of the base plate (see Figure 1b). The micropositioning system moving the microelectrode above the ATR crystal is part of a home-built SECM driven by stepper motors (Scientific Precision Instruments GmbH®, Oppenheim, Germany) with a precision of 0.02 μm. All electrochemical experiments were conducted with a CHI 842A bipotentiostat (CH Instruments, Inc., Austin, TX). The combined SECM-IR-ATR system was sealed into a darkened compartment and purged with nitrogen to avoid possible photopolymerization reactions of SNS, and to maintain stable atmospheric conditions for the IR measurements. The combined IR-ATR technique has been applied to simultaneously monitor an electropolymerization process locally induced by the SECM electrode via changes occurring in the IR spectrum appearing at different wavenumber regions, especially around 690 cm^{-1}.[57] All IR spectra obtained using the SECM-IR-ATR set-up were collected at a spectral resolution of 4 cm^{-1}, and by averaging 100 scans; the data were analyzed with the OPUS software package (Bruker Optics Inc., Billerica, MA).

UME preparation

Disk–shaped microelectrodes were fabricated as previously described by sealing a 25 μm (diam.) Pt wire under vacuum into a borosilicate glass capillary.[3] Successive grinding and polishing with diamond paste (6 μm and 3 μm) and with alumina paste (1 μm and 0.05 μm),

respectively, exposes a disk-shaped microelectrode. Cyclic voltammetry, optical microscopy, and AFM imaging were applied for characterizing the fabricated microelectrodes.

Chemicals

Deuterated water (D_2O), $Ru(bpy)_3Cl_2 \cdot 6H_2O$, KCl (reagent grade), and acetone (ACS spectrophotometric grade), were obtained from Sigma Aldrich (St. Louis, MO). Deionized water (Milli-Q water system, Millipore Corp., Billerica, MA) was used for preparing solutions if not stated otherwise. 0.02 M $Ru(bpy)_3Cl_2 \cdot 6H_2O$/0.1 M KCl electrolyte solution was prepared in D_2O. All solutions were deaerated by purging with UHP argon (Airgas, Hapeville, GA) prior to electrochemical experiments.

2,5-di-(2-thienyl)-pyrrole monomer was synthesized and purified based on the method described by Wynberg *et al*.[58] The precursor 1,4-bis(2-thienyl)butanedione was prepared following a procedure published by Stetter *et al*.59 The resulting 1,4-diketone was allowed to react with ammonium acetate, which resulted in the SNS derivative with a yield of 75 %.[58] 2,5-di-(2-thienyl)-pyrrole was purified and stored under argon. 0.1 M SNS was dissolved in acetone and drop-casted on the ATR crystal surface.

Ex-situ FT-IR studies on SNS monomer and electrogenerated poly(SNS)

A three-electrode configuration with a Pt sheet (1 cm^2) as working electrode, a Pt mesh (effective area 10 cm^2) auxiliary electrode, and an Ag/AgCl quasi reference electrode was used for macroscopic poly(SNS) deposition. Both Pt sheet and Mesh were flame-burned prior to usage. The Pt sheet was coated with SNS monomer, and then immersed into 0.1 M KCl aqueous solution. Prior to the deposition, cyclic voltammetry was performed in a potential range of 0-1.2 V (*vs*. Ag/AgCl) at a scan rate of 0.1 V/s to determine the oxidation rate of the monomer. A constant potential of 1.0 V *vs*. Ag/AgCl was applied to the Pt sheet for 2, 5, or 10 min to polymerize SNS in a series of experiments. The obtained thickness of poly(SNS) films was approx. around 2 μm for all conducted experiments. Different degrees of polymerization were achieved by varying the deposition time. Excess SNS monomer at the Pt sheet after polymerization was removed in methanol during sonication of the substrate. IR absorption spectra of the adsorbed SNS monomer film prior to polymerization, and poly(SNS) films generated at different polymerization times were collected using a nitrogen purged Equinox 55 FT-IR spectrometer (Bruker Optics Inc., Billerica, MA). All IR spectra were collected at a spectral resolution of 4 cm^{-1}, and by averaging 100 scans. Analysis of the spectra was performed using the OPUS software package.

SECM feedback mode polymerization of SNS

0.1 M SNS monomer solution was coated onto the surface of a ZnSe crystal (~1 cm × 1 cm) by drop-casting prior to fixing the SNS-modified ZnSe in a conventional SECM electrochemical cell. A three-electrode assembly using a 25 μm Pt disk UME as working electrode, a Pt wire auxiliary electrode, and an Ag/AgCl wire reference electrode was used for all SECM experiments. The cell was filled with 0.02 M $Ru(bpy)_3Cl_2$/0.1 M KCl/D_2O. SECM approach curves at a potential of 1.0 V *vs*. Ag/AgCl were recorded, and the approach of the UME towards the SNS-coated ZnSe crystal was stopped when the steady state current had increased by 20 % compared to steady state current at the UME in bulk solution. Poly(SNS) spots were formed at different locations at the ZnSe crystal surface by applying a constant potential of 1.0 V *vs*. Ag/AgCl to the UME. At this potential, the mediator $Ru(bpy)_3^{2+}$ is oxidized to $Ru(bpy)_3^{3+}$, which diffuses to the ZnSe crystal if the UME is in close proximity to the sample surface. $Ru(bpy)_3^{3+}$ is driving the oxidation of the adsorbed SNS monomer forming a radical cation ($SNS^{\cdot+}$), which is followed by a condensation reaction of $SNS^{\cdot+}$ to the dimer. Chain propagation leads to oligomers, and finally to poly(SNS), as shown in Figure 1c.[60]

Simultaneous IR-ATR studies on microstructured poly(SNS) formed by SECM

The SNS monomer film was deposited onto the surface of the hemispheric ZnSe ATR crystal by drop-casting from 0.1 M SNS acetone solution. Electropolymerization was obtained by feedback mode SECM in 0.02 M $Ru(bpy)_3Cl_2$/0.1 M KCl/D_2O solution, as described above. The UME tip was approached to the sample surface by monitoring the feedback current, and stopped once the current at the tip increased by 20 % compared to the current in bulk solution. *In-situ* evanescent field IR absorption spectra were collected during the progress of feedback mode SECM polymerization reactions at different time intervals (5, 10, 20, and 30 min). In addition, micropatterning of multiple polymer spots *via* electropolymerization at the hemispherical ZnSe ATR crystal surface using SECM was simultaneously monitored by *in-situ* evanescent field IR absorption measurements. The UME was positioned closely to the center of SNS/hemispheric ZnSe, and was then moved at constant height to five discrete locations at the ATR crystal surface. At each location, the UME was held stationary for 20 min allowing for polymerization of adsorbed SNS. An IR spectrum was collected at the end of each individual polymerization step. Prior to SNS monomer film coating at the ATR crystal surface, a background IR spectrum in nitrogen atmosphere was recorded using the bare crystal. In addition, prior to combined SECM-IR-ATR experiments *in-situ* monitoring of the electropolymerization process was performed via IR studies using macroscopic Pt electrodes (1 mm) for electrochemically induced deposition at the single bounce ATR crystal. The macroscopic electrode was positioned at a distance of approx. 100 μm from the SNS-modified ATR crystal prior to initiation of the electropolymerization, and remained at this position there until no further IR signal change during the electropolymerization process was observed.

Results and discussion

FT-IR studies on SNS monomer and electrogenerated poly(SNS)

A number of papers have been published studying the electrochemical properties of SNS in organic[61-64] or in mixtures of water with organic solvents[65] containing appropriate supporting electrolytes. Cyclic voltammetry was applied to study the electrochemical properties of SNS in aqueous solution. SNS monomer was coated onto a Pt sheet and immersed in 0.1 M KCl aqueous solution. The electrochemical results obtained from these experiments are consistent with literature data obtained by electrogenerated polymerization of SNS. FT-IR studies have been performed to identify the primary polymerization position(s), and the time-dependence of the polymerization level of SNS. Figure 2a shows the spectral changes of the IR absorption spectra with respect to the polymerization time. The out-of-plane C-H bending vibrations in the spectral region of 600-1600 cm^{-1} were analyzed for characterizing the SNS polymerization level. C-H IR absorptions characteristic for the different hydrogens positioned at the thiophene and pyrrole unit of the SNS monomer are determined as follows: α-H has an IR absorption around 690 cm^{-1}, β-H and β'-H around 842 cm^{-1}, and β”-H around 770 cm^{-1}.[57, 64] As evident, during the polymerization process the relative peak intensity for α-H decreases. In addition, a peak around 800 cm^{-1} attributed to β”-H emerges, and its intensity increases with progress of the polymerization due to flanking of the middle pyrrole ring of SNS in poly(SNS). Furthermore, weaker absorption peaks appear in the higher frequency region of the fingerprint regime (850-900 cm^{-1}), which are related to β-H and β'-H vibrations at the end of the polymer chain. Based on the obtained polymerization time dependent spectra, it is concluded that the SNS polymerization in aqueous solution primarily occurs at the α position, and hence, the intensity change of the characteristic α-H vibrational mode may be used for monitoring the polymerization level during SECM-IR-ATR studies.

SECM feedback mode polymerization of SNS

SNS was coated onto the ATR crystal surface, and the SECM electrode tip was approached to the ATR crystal surface by monitoring the feedback current. Tip-generated $Ru(bpy)_3^{3+}$

subsequently oxidizes SNS monomer at the surface forming an intermediate radical cation ($SNS^{\cdot+}$), which is followed by dimer formation via condensation of $SNS^{\cdot+}$ radicals. As the chain reaction progresses, oligomers, and finally poly(SNS) are formed, as schematically shown in Figure 1c.[60] After feedback mode induced polymerization, the SNS/ZnSe was rinsed with DI H_2O und acetone, respectively. As expected, well-defined poly(SNS) spots were generated, as shown in the optical microscopy image shown in Figure 2b. Fig. 2b reveals that the poly(SNS) spot sizes increase with time of electropolymerization. The generated polymer spots ranged in diameter from 180 to 210 μm corresponding to polymerization times ranging from 5 to 20 min, respectively. The dimension of the obtained spots compare with the dimensions of the entire UME (active electrode and glass insulation), which is related to the diffusion of the redox mediator $Ru(bpy)_3^{3+}$ and the SNS radical cations, the distance between UME and SNS/ZnSe, the kinetics of involved surface reactions, and the electrochemical reaction time.[3]

In-situ IR-ATR studies of surface modifications induced by feedback mode SECM

Prior to the polymerization reaction, the thickness of the adsorbed SNS film at the hemispherical ZnSe ATR crystal was determined by AFM measurements. The average thickness was determined at 200-400 nm. The stability of the SNS film coated onto the hemispherical ZnSe ATR crystal surface was monitored via IR-ATR during a period of 8 h after coating the crystal already within the combined SECM-IR-ATR set-up, which was purged with nitrogen. No change of the IR signal was observed for this period indicating a stable monomer layer. All *in-situ* electrochemical experiments were conducted in deuterated water, as D_2O provides an IR transparent window in the region of 660 – 1000 cm^{-1}, which is the spectral region of interest providing access to the IR absorption features relevant for monitoring the polymerization progress of SNS.

Prior to microstructuring the SNS monomer film via SECM, a 1 mm Pt electrode was positioned at a close distance (approx. 100 μm) to the SNS-modified ZnSe crystal surface. By applying a potential of 1 V *vs*. Ag/AgCl in 0.02 M $Ru(bpy)_3Cl_2$/0.1 M KCl/D_2O, the current rapidly increased and then dropped to the bulk current after approx. 2 min. Figure 3 shows the IR spectra of the SNS film prior to and after 2 min of electropolymerization. After this period, no further detectable changes in the IR spectra were determined. After rinsing with DI water and acetone, a dark poly(SNS) spot with a diameter of approximately 1.8 mm in visible at the surface of the hemispherical ATR crystal. The IR data obtained from this experiment are in agreement with the data presented in Fig. 2a showing *ex-situ* FT-IR results obtained from the SNS monomer and electrogenerated poly(SNS).

Three consecutive *in-situ* polymerization experiments using the combined IR-ATR-SECM set-up were performed. A representative data set of the IR measurements for a polymerization sequence in the region of 670-710 cm^{-1}, presenting the out of the plane α-H bending vibration is shown in Fig. 4. The α-H peak areas were integrated from 670 cm^{-1} to 710 cm^{-1}, and the polymerization levels for different reaction times were calculated by determining the percentage of peak area change between the integrated α-H peak area of polymerized SNS at the different polymerization times, and the integrated α-H area of the SNS monomer. Thus obtained polymerization levels for three sets of experiments are presented in Table 2. AFM studies and optical microscopy images revealed that the monomer film thickness is not homogeneous; the film thickness ranged from 200-400 nm with ridges and flat regions, which are formed during film adsorption. Hence, the resulting poly(SNS) films may have different thicknesses and different levels of polymerization yet during the same observation periods for the IR measurements. Furthermore, the IR measurement is subject to intensity variations across the ZnSe single bounce crystal surface in dependence of the area illuminated by the evanescent

field.[66] These factors are considered responsible for the fact that despite keeping the conditions for polymerizing each spot constant, variations in the IR signal are still observable.

Figure 5 shows the results for *in-situ* IR-ATR monitoring of the formation of six poly(SNS) spots induced by feedback mode SECM. The scheme in the insert shows the relative position and deposition sequence of the spots. The α-H peak areas were integrated from 670 cm^{-1} to 710 cm^{-1}, and the overall polymerization levels after each polymer spot deposition were calculated by determining the percentage of peak area change between the integrated α-H area of poly(SNS), and the integrated α-H area of the SNS monomer signal. Thus calculated polymerization levels are summarized in Table 3. The differences in polymerization level between two adjacent polymer spot depositions are also listed in Table 3. As previously discussed, from the data in Table 3 it is evident that the integrated area of the characteristic peaks shows some variation between adjacent spots. In particular, the deposition at spot 2, which resulted in a change of 17% is significantly higher compared to the other spots. These variations are attributed to the difference in evanescent field sensitivity across the ATR crystal at different surface locations, or to inhomogeneity of the pre-deposited SNS monomer film. It is however anticipated that the next-generation combined SECM-IR-ATR instrument currently developed by our research group will provide for a uniform evanescent field across the entire sensing interface based the introduction of advanced planar waveguide technologies currently developed at our research group[67, 68] in lieu of the single-bounce ATR crystal, thereby significantly improving the reproducibility of the IR signal.

Conclusions

We present the first instrumental combination of scanning electrochemical microscopy (SECM) with *in-situ* attenuated total reflection infrared spectroscopy (IR-ATR) using a single bounce ATR crystal as SECM substrate. The capabilities of the SECM-IR-ATR were demonstrated by simultaneously spectroscopically monitoring the microstructured electropolymerization of 2,5-di-(2-thienyl)-pyrrole, which was induced by feedback mode SECM. The level of polymerization could be evaluated by the recorded IR spectra, which were synchronized with the progression of the electrochemically-induced polymerization. Furthermore, access to the fingerprint region of the IR spectrum (> 10μm) not only revealed the polymerization level but provided direct spectroscopic insight on the polymerization mechanism, which was verified via *ex-situ* data and reports in literature.

Future research is targeted towards next-generation SECM-IR-ATR technology using planar waveguides providing uniform evanescent field intensity, and towards combining AFM techniques with SECM-IR-ATR by using bifunctional AFM-SECM probes. This triple combination AFM-SECM-IR-ATR will provide a unique multifunctional analytical platform enabling simultaneous *in-situ* studies on topographic (AFM), infrared spectroscopic (IR-ATR), and electrochemical (SECM) processes.

Acknowledgments

The authors acknowledge S.-S. Kim and A. Wilk for fruitful discussions. Financial support by the National Institutes of Health, NIH (R01-EB000508) is greatly acknowledged.

References

1. Wittstock G, Burchardt M, Pust SE, Shen Y, Zhao C. Angew. Chem. Int. Ed 2007;46:1584–1617.
2. Sun P, Laforge FO, Mirkin MV. Phys. Chem. Chem. Phys 2007;9:802–823. [PubMed: 17287874]
3. Bard, AJ.; Mirkin, MV. Scanning Electrochemical Microscopy. Marcel Dekker; New York: 2001.
4. Ammann E, Mandler D. J. Electrochem. Soc 2001;148:C533–C539.

5. Cliffel DE, Bard AJ. Anal. Chem 1998;70:1993–1998.
6. Husser OE, Craston DH, Bard AJ. J. Electrochem. Soc 1989;136:3222–3229.
7. Kranz C, Gaub HE, Schuhmann W. Adv. Mater 1996;8:634–637.
8. Kranz C, Ludwig M, Gaub HE, Schuhmann W. Adv. Mater 1995;7:38–40.
9. Ku S-Y, Wong K-T, Bard AJ. J. Am. Chem. Soc 2008;130:2392–2393. [PubMed: 18251478]
10. Lin CW, Fan FRF, Bard AJ. J. Electrochem. Soc 1987;134:1038–1039.
11. Mandler D, Bard AJ. J. Electrochem. Soc 1989;136:3143–3144.
12. Mandler D, Bard AJ. J. Electrochem. Soc 1990;137:2468–2472.
13. Mandler D, Bard AJ. J. Electrochem. Soc 1990;137:1079–1086.
14. Meltzer S, Mandler D. J. Electrochem. Soc 1995;142:L82–L84.
15. Meltzer S, Mandler D. J. Chem. Soc., Faraday Trans 1995;91:1019–1024.
16. Nowall WB, Wipf DO, Kuhr WG. Anal. Chem 1998;70:2601–2606. [PubMed: 9666728]
17. Shiku H, Takeda T, Yamada H, Matsue T, Uchida I. Anal. Chem 1995;67:312–317.
18. Shiku H, Uchida I, Matsue T. Langmuir 1997;13:7239–7244.
19. Shohat I, Mandler D. J. Electrochem. Soc 1994;141:995–999.
20. Wittstock G, Hesse R, Schuhmann W. Electroanalysis 1997;9:746–750.
21. Craston DH, Lin CW, Bard AJ. J. Electrochem. Soc 1988;135:785–786.
22. Wuu YM, Fan FRF, Bard AJ. J. Electrochem. Soc 1989;136:885–886.
23. Kranz C, Ludwig M, Gaub HE, Schuhmann W. Adv. Mater 1995;7:568–571.
24. Zhou J, Wipf DO. J. Electrochem. Soc 1997;144:1202–1207.
25. Borgwarth K, Rohde N, Ricken C, Hallensleben ML, Mandler D, Heinze J. Adv. Mater 1999;11:1221–1226.
26. Hess C, Borgwarth K, Ricken C, Ebling DG, Heinze J. Electrochim. Acta 1997;42:3065–3073.
27. Turyan I, Krasovec UO, Orel B, Saraidorov T, Reisfeld R, Mandler D. Adv. Mater 2000;12:330–333.
28. Borgwarth K, Rohde N, Ricken C, Hallensleben ML, Mandler D, Heinze J. Adv. Mater 1999;11:1221–1226.
29. Zhou J, Wipf DO. J. Electrochem. Soc 1997;144:1202–1207.
30. Li X, Geng Q, Wang Y, Si Z, Jiang W, Zhang X, Jin W. Electrochim. Acta 2007;53:2016–2024.
31. Sugimura H, Uchida T, Kitamura N, Shimo N, Masuhara H. J. Electroanal. Chem 1993;361:57–63.
32. Widrig CA, Chung C, Porter MD. J. Electroanal. Chem. Interfacial Electrochem 1991;310:335–359.
33. Wittstock G, Schuhmann W. Anal. Chem 1997;69:5059–5066.
34. Yang DF, Wilde CP, Morin M. Langmuir 1996;12:6570–6577.
35. Treutler TH, Wittstock G. Electrochim. Acta 2003;48:2923–2932.
36. Williams DE, Mohiuddin TF, Zhu YY. J. Electrochem. Soc 1998;145:2664–2672.
37. Garfias-Mesias LF, Smyrl WH. J. Electrochem. Soc 1999;146:2495–2501.
38. Fasching RJ, Tao Y, Prinz FB. Sens. Actuators, B 2005;B108:964–972.
39. Gullo MR, Frederix PLTM, Akiyama T, Engel A, de Rooij NF, Staufer U. Anal. Chem 2006;78:5436–5442. [PubMed: 16878880]
40. Kranz C, Friedbacher G, Mizaikoff B, Lugstein A, Smoliner J, Bertagnolli E. Anal. Chem 2001;73:2491–2500. [PubMed: 11403290]
41. Macpherson JV, Unwin PR. Anal. Chem 2000;72:276–285. [PubMed: 10658320]
42. Gollas B, Bartlett PN, Denuault G. Anal. Chem 2000;72:349–356. [PubMed: 10658330]
43. Hess C, Borgwarth K, Heinze J. Electrochim. Acta 2000;45:3725–3736.
44. Shin M, Jeon IC. Bull. Korean Chem. Soc 1998;19:1227–1232.
45. Lee Y, Bard AJ. Anal. Chem 2002;74:3626–3633. [PubMed: 12175146]
46. Maruyama K, Ohkawa H, Ogawa S, Ueda A, Niwa O, Suzuki K. Anal. Chem 2006;78:1904–1912. [PubMed: 16536427]
47. Evju JK, Smyrl WH. Proceedings - Electrochemical Society 2001;2001-22:181–192.
48. Boldt F-M, Heinze J, Diez M, Petersen J, Boersch M. Anal. Chem 2004;76:3473–3481. [PubMed: 15228313]

49. Fan F-RF, Cliffel D, Bard AJ. Anal. Chem 1998;70:2941–2948.
50. Kanoufi F, Cannes C, Zu Y, Bard AJ. J. Phys. Chem. B 2001;105:8951–8962.
51. Miao W, Choi J-P, Bard AJ. J. Amer. Chem. Soc 2002;124:14478–14485. [PubMed: 12452725]
52. Szunerits S, Walt DR. ChemPhysChem 2003;4:186–192. [PubMed: 12619418]
53. Szunerits S, Knorr N, Calemczuk R, Livache T. Langmuir 2004;20:9236–9241. [PubMed: 15461512]
54. Brucherseifer M, Kranz C, Mizaikoff B. Anal. Chem 2007;79:8803–8806. [PubMed: 17939644]
55. Harrick, NJ. Internal reflection spectroscopy. Interscience Publishers; New York: 1967.
56. Dobbs GT, Balu B, Young C, Kranz C, Hess DW, Mizaikoff B. Anal. Chem 2007;79:9566–9571. [PubMed: 18020310]
57. Ferraris JP, Hanlon TR. Polymer 1989;30:1319–1327.
58. Wynberg H, Metselaar J. Synth. Commun 1984;14:1–9.
59. Stetter H. Angew. Chem 1976;88:695–704.
60. Niziurski-Mann RE, Scordilis-Kelley C, Liu TL, Cava MP, Carlin RT. J. Am. Chem. Soc 1993;115:887–891.
61. Ferraris JP, Skiles GD. Polymer 1987;28:179–182.
62. Brillas E, Carrasco J, Figueras A, Urpi F, Otero TF. J. Electroanal. Chem 1995;392:55–61.
63. Otero TF, Carrasco J, Figueras A, Brillas E. Synth. Met 1996;83:193–196.
64. Brillas E, Carrasco J, Oliver R, Estrany F, Ruiz V. Collect. Czech. Chem. Commun 1999;64:1357–1368.
65. Carrasco J, Brillas E, Fernandez V, Cabot P-L, Garrido JA, Centellas F, Rodriguez RM. J. Electrochem. Soc 2001;148:E19–E25.
66. Dobbs GT, Mizaikoff B. Appl. Spectrosc 2006;60:573–583. [PubMed: 16808857]
67. Charlton C, Giovannini M, Faist J, Mizaikoff B. Anal. Chem 2006;78:4224–4227. [PubMed: 16771554]
68. Charlton C, Katzir A, Mizaikoff B. Anal. Chem 2005;77:4398–4403. [PubMed: 16013852]

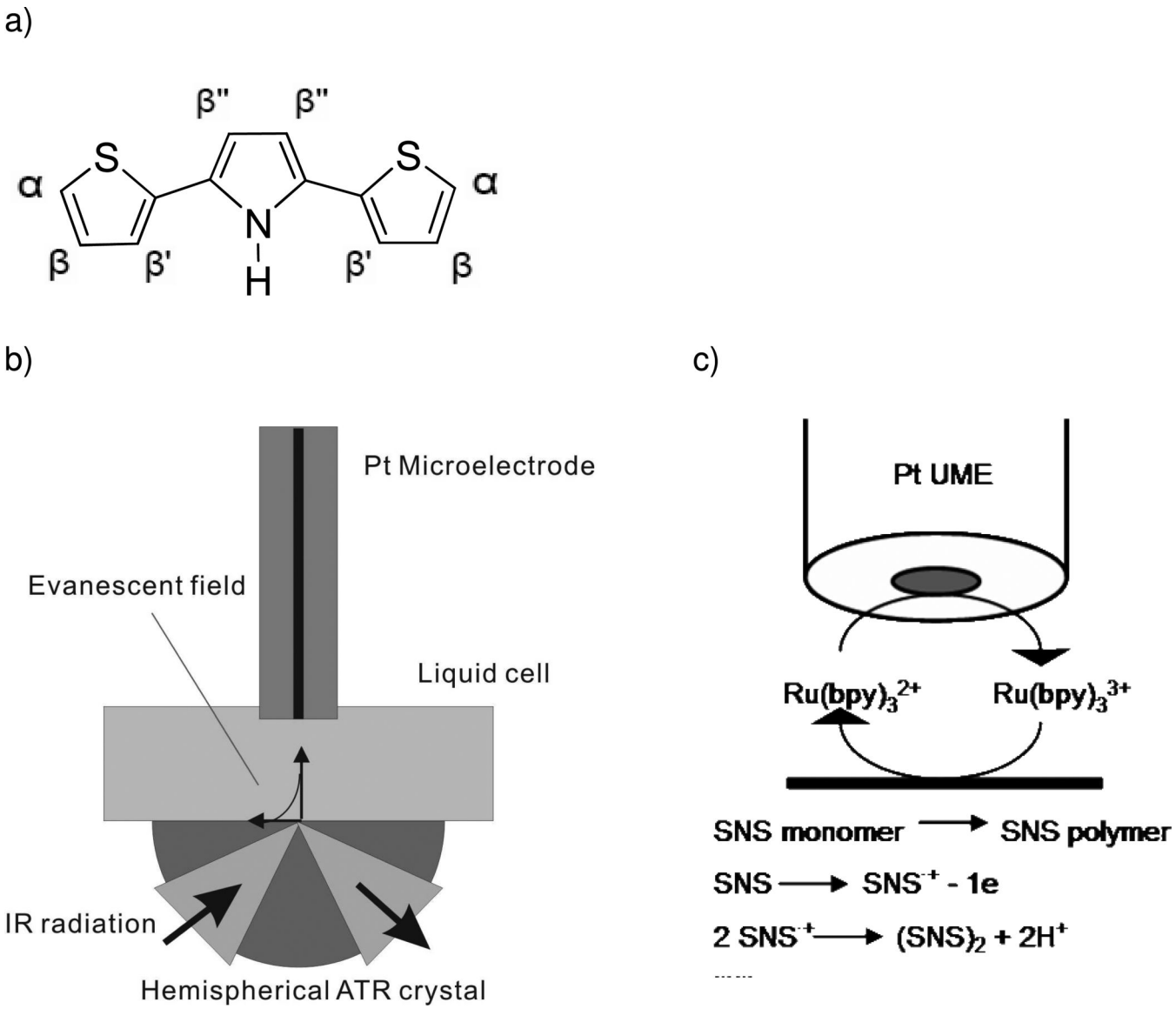

Figure 1.

(a) 2,5-di-(2-thienyl)-pyrrole (SNS) structure with labeled hydrogen atoms; (b) Scheme of the SECM-ATR-FTIR set-up; (c) SNS polymerization through feedback mode SECM using Ru $(bpy)_3^{2+}$ as mediator.

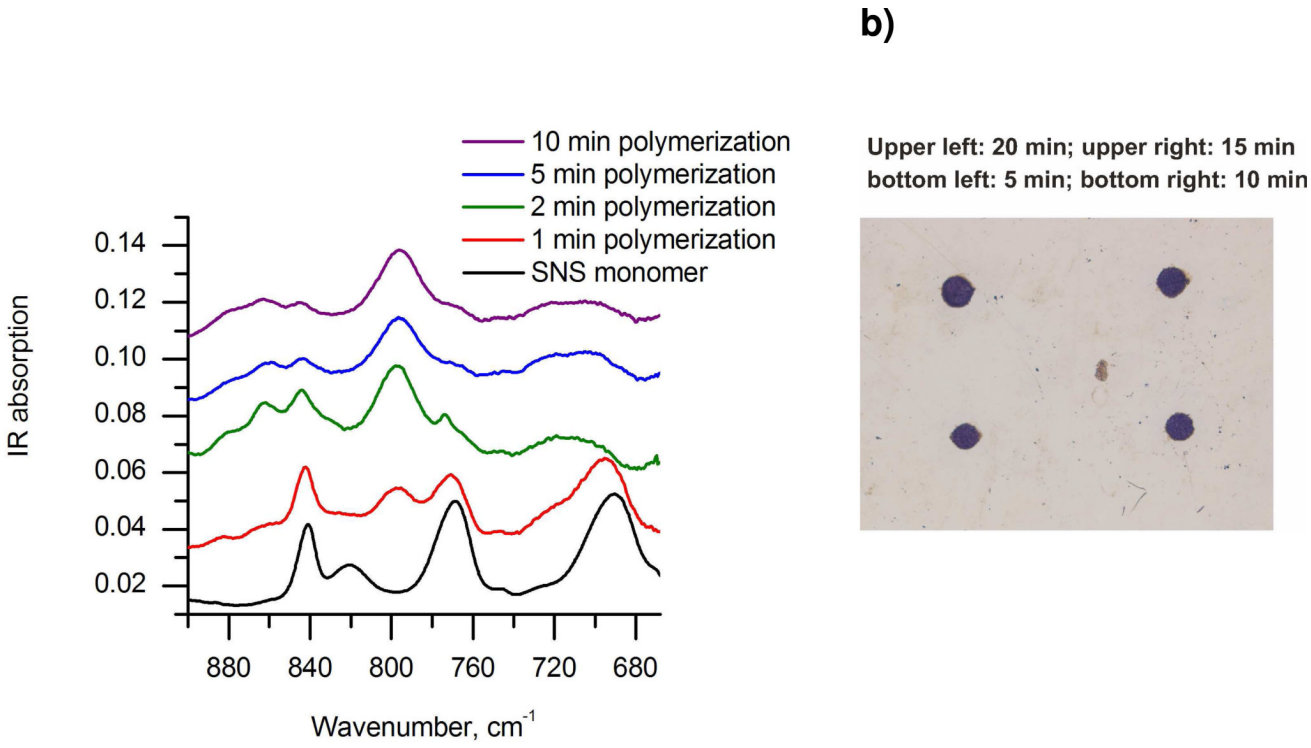

Figure 2.

a) *Ex-situ* IR characterization of poly(SNS) formed on a Pt sheet electrode during progressing electropolymerization. b) Optical micrograph of poly(SNS) spots formed at the ZnSe crystal surface during different electropolymerization periods: upper left – 20 min; upper right – 15 min; bottom left – 5 min; bottom right – 10 min.

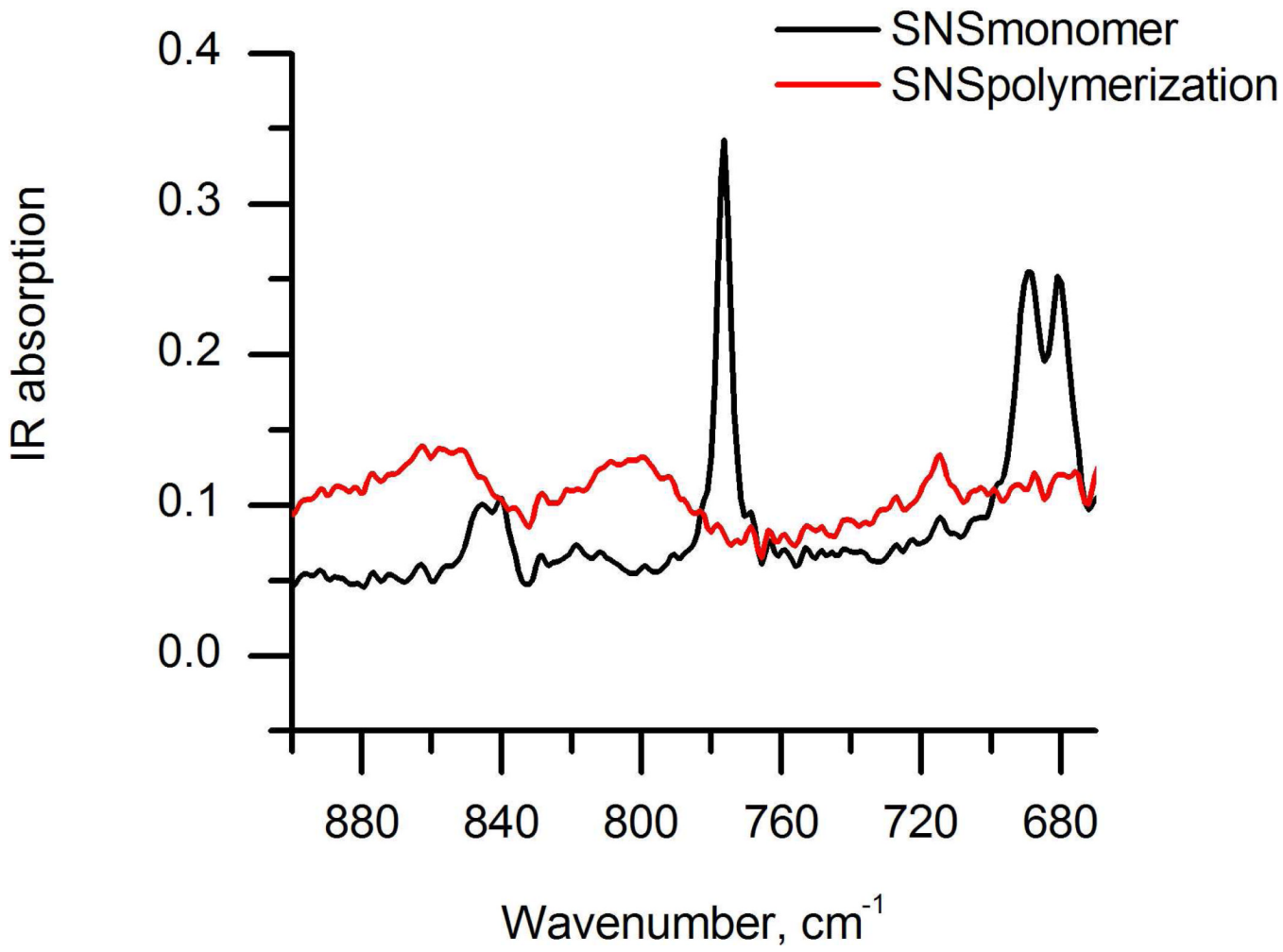

Figure 3.
Simultaneous *in-situ* IR-ATR characterization of SNS polymerization induced via a 1 mm Pt disk electrode.

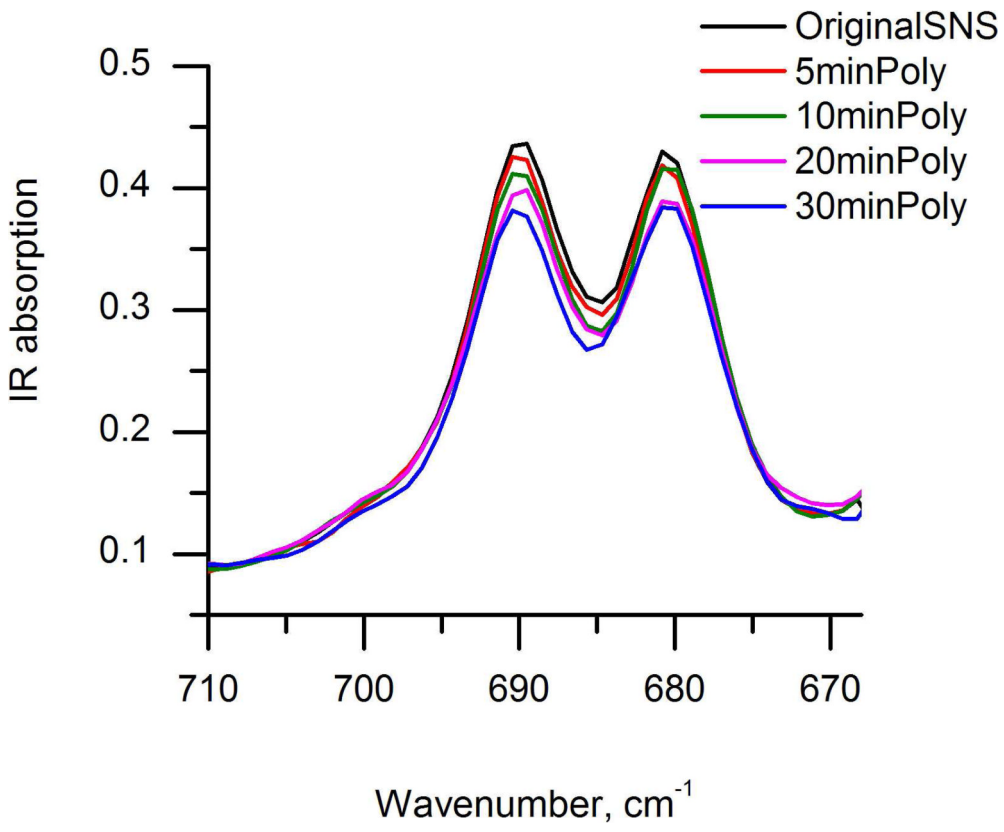

Figure 4.
Simultaneous *in-situ* IR-ATR characterization of SNS polymerization induced via feedback-mode SECM using a 25μm Pt ultramicroelectrode.

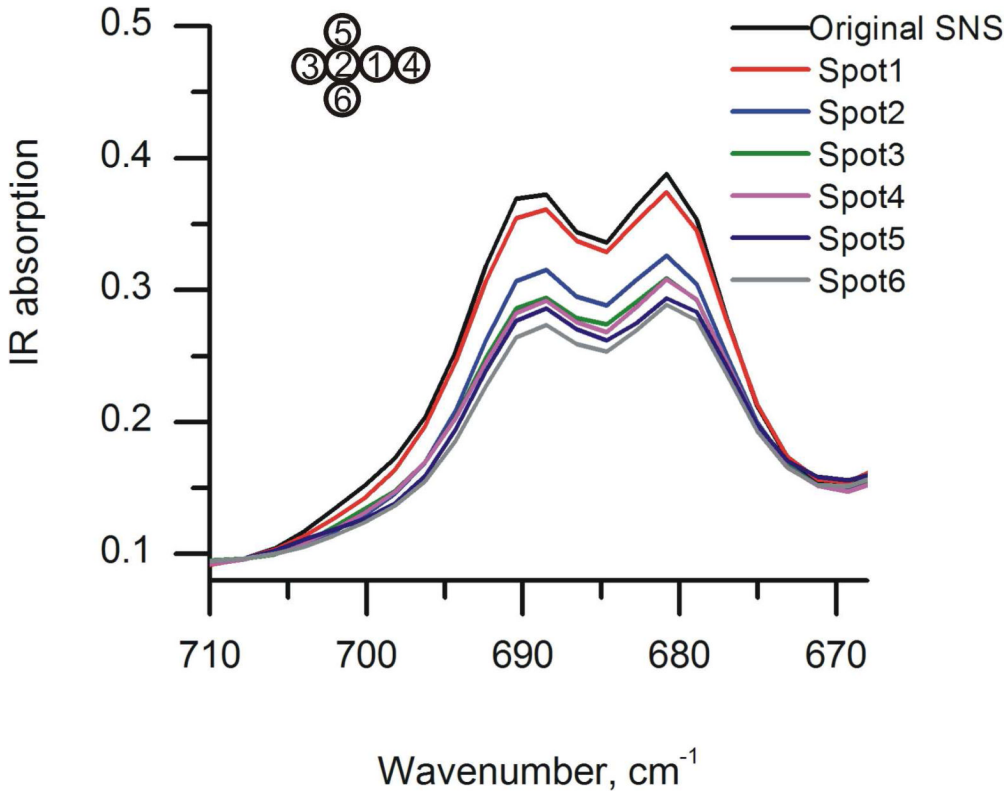

Figure 5.
Simultaneous *in-situ* IR-ATR characterization of poly(SNS) patterning at different spots via feedback-mode SECM using a 25μm Pt ultramicroelectrode.

Table 1

Changes of the Poly(SNS) spot size with respect to the polymerization time.

Polymerization time [min]	5	10	15	20
Deposited spot size [μm]	180	190	200	205

Table 2

Changes of the polymerization level calculated from integrated α-H peak area of polymerized SNS and the integrated α- H area of SNS monomer (integrated from 670 cm^{-1} to 710 cm^{-1}) in respect to polymerization time. Three sets of time-dependant *in-situ* electropolymerization of SNS are presented (experiment 1 -3). The peak area change of the polymerization levels are presented in %.

Polymerization time [min]	α-H polySNS vs. SNS peak area change [%] Exp. 1	α-H polySNS vs. SNS peak area change [%] Exp. 2	α-H polySNS vs. SNS peak area change [%] Exp. 3
5	2.78	3.19	5.72
10	8.64	9.31	13.4
20	15.7	17.1	21.2
30	19.1	23.4	26.5

Table 3

Changes of overall polymerization level with respect to polymerization location and the differences of polymerization levels between two adjacent polymerization spots obtained from the percentage of peak area change of the integrated α-H peak area of polymerized SNS and the integrated α- H area of SNS monomer. Unit: %.

	Deposited spot 1	Deposited spot 2	Deposited spot 3	Deposited spot 4	Deposited spot 5	Deposited spot 6
Cumulative peak area change α-H polySNS/SNS [%]	6.35	23.8	30.2	30.6	36.1	39.3
Spot-to-spot peak area change α-H polySNS/SNS $\Delta(Poly_i - Poly_{i-1})$ [%]	6.35	17.5	6.4	0.5	5.5	3.2